Hydrology Research

Urbanization effects on the groundwater potential recharge of the aquifers in the southern part of the Basin of Mexico

José Roberto Ávila-Carrasco[a], Mario Alberto Hernández-Hernández IWA iD [b],*, Graciela S. Herrera[c] and Guillermo De Jesús Hernández-García[c]

[a] Facultad de Ingeniería, Departamento de Hidráulica, Universidad Nacional Autónoma de México (UNAM), Circuito de la Investigación Científica SN, Ciudad Universitaria, Coyoacán CP 04510, Mexico
[b] Cátedras CONACYT – Instituto de Geofísica, Universidad Nacional Autónoma de México (UNAM), Circuito de la Investigación Científica SN, Ciudad Universitaria, Coyoacán CP 04510, Mexico
[c] Instituto de Geofísica, Universidad Nacional Autónoma de México (UNAM), Circuito de la Investigación Científica SN, Ciudad Universitaria, Coyoacán CP 04510, Mexico
*Corresponding author. E-mail: malbher@igeofisica.unam.mx

iD MAH-H, 0000-0002-1892-3511

ABSTRACT

Collection, processing, and analysis of GIS and satellite data were performed in this work to estimate temporal groundwater recharge changes, which are needed as input in numerical groundwater-flow models. Layers of geological alignments, land use, drainage network, lithology, topography, and precipitation were collected. This information was spatialized, then layer importance was calculated using an Analytic Hierarchy Process (AHP) based on infiltration capacity to define Potential Recharge (PR) regions. A water budget equation was used to calculate PR volumes. The analysis was done every five years from 1970-19, considering average urban area changes. For all study periods, an increase in urban area was calculated from 16 to 28% of the total study area, while potential recharge decreased from 23 to 19% of the mean precipitation values for each 5-year period. The most significant urban expansion was from 1980-94 and 2010-19, which match periods of potential recharge decrease. However, a slight increase in PR from 2000-09, unrelated to urban area change, may be due to temperature variations. The results account for the spatial and temporal dynamics of the recharge in the study area and can be used as input data to calibrate the actual recharge in a groundwater numerical model.

Key words: hierarchical analysis process, potential groundwater recharge, satellite images, sustainable management

HIGHLIGHTS

- Urban development has triggered natural groundwater recharge depletion.
- Potential recharge was estimated for the Mexico City groundwater supply area.
- AHP and GIS weighting overlay were used to map groundwater potential recharge.
- A surface water balance was applied to calculate recharge volumes for 5-year periods from 1970 to 2019.
- The estimated potential recharge showed a decrease of 18% along the entire period of analysis.

GRAPHICAL ABSTRACT
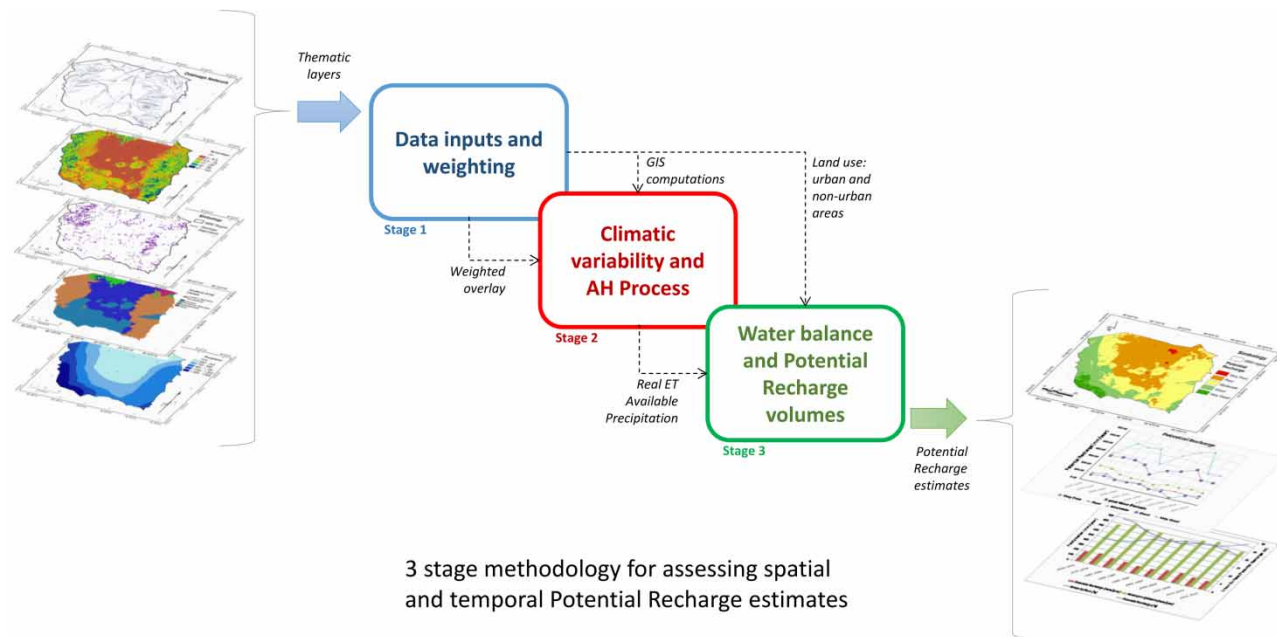
INTRODUCTION

The growing water pressure caused by the disproportionate increase in population and urbanization in large cities has triggered several adverse effects on groundwater resources. A common effect is the reduction of the natural recharge (produced by rainfall) of the underlying aquifer due to changes in land use/cover, overexploitation, and changes in the precipitation regime. Impact quantification of land use temporal changes is essential to develop groundwater-flow models and generate management programs. For example, Adhikari *et al.* (2020) analyzed the effects of growing urban Ho Chi Minh City on groundwater recharge, evaluated three future scenarios up to the year 2100 of the low, medium, and high urbanization using an empirical land use projection model and a hydrological SWAT model. They found that an increase in the urban area significantly impacts recharge, reducing it by 30 and 52% in medium and high urbanization, respectively. Another issue is the combined impact of climate change and land use change on groundwater recharge (see, for example, Ghimire *et al.* 2021; BuhayBucton *et al.* 2022). Recharge could be any infiltrated water that reaches the water table, but it may return to the atmosphere by evapotranspiration or remain in the unsaturated zone. According to Healey & Scanlon (2010), infiltrating water can be viewed as potential recharge, so for the rest of the document, both terms will be used interchangeably.

Actualized land use cover change (LUCC) maps are needed to estimate potential groundwater recharge (PGR) but are challenging to develop, especially in developing countries. However, technological advancement, satellite images, and software make it possible to integrate remote sensing (RS) techniques and geographic information systems (GIS) to support recharge estimation. Suganthi *et al.* (2013) delineated potential groundwater zones using combined RS-GIS systems, overlaying lithology, geomorphology, slope, geologic lineaments, drainage, and precipitation maps, to better plan groundwater use in the city of Chennai, India. Oikonomidis *et al.* (2015) evaluated groundwater recharge potential with RS-GIS in Thessaly, Greece; the recharge potential varied from very high to very low, using and assigning weights to similar thematic layers, including potential recharge and piezometric levels; this allowed them to generate water quality suitability maps. Similarly, Rwanga & Ndambuki (2017) and Wang *et al.* (2008) used RS-GIS to perform potential recharge calculations. However, they did not address the temporal recharge component caused by the change in land use associated with urban growth.

On the other hand, Guerrero-Morales *et al.* (2020) evaluated the proportional variation in PGR due to urbanization and climate change in Acapulco, Mexico, where LUCC forecasts, supervised classification of land use images, and a Markov model was used to predict LUCC to 2050. The results indicated recharge losses of 73 and 273 Mm³ in 2017 and 2050, respectively. LUCC is intrinsically related to runoff rates, and several authors have recently applied the runoff coefficient to complete

the components in water budgets at unmonitored basins. Peng (2019) introduced a new approach to reconstructing runoff records at large lakes' ungauged basins, using various components of the water budget. Son & Kwon (2022) analyzed increasing the infiltration rate of rainwater by analyzing the water budget and estimating the runoff coefficient in urban parks.

Mexico City Metropolitan Zone is located in the southern part of the Basin of Mexico (SBM). The urban development has triggered environmental problems, including the upper aquifer overexploitation and reduced recharge zones in the south and southwest of the basin. The Mexican National Commission of Water (CONAGUA, Spanish acronym) has divided the SBM into three administrative aquifers according to hydrogeological and administrative criteria: 'Mexico City Metropolitan Zone (ZMCM, Spanish acronym)', 'Texcoco', and 'Chalco-Amecameca'. Development of conceptual models is essential at the beginning of any recharge study. These models can be adjusted as additional data provide new insights into the hydrologic system and may indicate where, when, and why recharge occurs. The main components of conceptual models are influencing factors and water budgets that provide a link between recharge and other processes. Some studies partially analyze the recharge in the SBM. Carrera-Hernández & Gaskin (2008) estimated groundwater recharge through daily water budgets, considering different vegetation and soil types, topography, and climate. Results indicated that recharge occurs mainly in mountainous regions, suggesting that although recharge has diminished in the alluvial plain, urban growth in the SBM has a minimal impact. However, this study covers a short period (1975–1986) and does not consider important local geological aspects such as lithology. Later, Gómez-Reyes (2013) presented a methodology to obtain the water components in hydrographic basins to assess the input and output water volumes using geographical and statistical data. Ruiz (2015) applied water table fluctuation methods and groundwater-flow modeling to evaluate spatiotemporal recharge in the area. The results revealed a variation in mean annual recharge greater than the precipitation that generated it, from 20% in the mountains to 3% in the plains. Meanwhile Peña-Díaz (2019) applied a methodology that accounts for surface water and groundwater to assess recharge availability, using successive approximations to get potential recharge coefficients for the upper aquifer but focusing mainly on high areas.

Other studies that include an integrated conceptual model are those of 'Sistema de Aguas de la Ciudad de México' (SACMEX 2005), which determined recharge between 1970 and 2003 considering land use by associating respective runoff coefficients and using a water budget. The results suggested a significant decreasing recharge trend attributed to increased temperatures and reduced precipitation. However, this study was carried out by administrative delegations and municipalities without considering governing parameters that affect potential recharge in the study area. Boyás Martínez et al. (2021) mapped zones of potential artificial recharge using categories from very poor to very good. They used a multiple influence factor (MIF) approach to assign weights to priority variables, such as lithology and land use. The results indicate that mountain ranges such as 'El Ajusco' and 'Chichinautzin' have the most significant potential recharge; however, essential parameters obtained with remote sensors, such as geological alignments and land use maps, are not included. Furthermore, the technique for assigning weights downplays precipitation, a priority variable. Mautner et al. (2020) carried out a multi-objective analysis to evaluate aquifer management alternatives focusing on flood risk analysis on urbanized ZMCM. They used a groundwater-flow model and incorporated trends in land use, repairs to the water supply distribution network, an increase in wastewater treatment, potential recharge, and imported water potential recharge. However, this study mainly focuses on urban groundwater systems regardless of other essential surface factors.

This work aims to develop a conceptual model of recharge processes and estimate potential recharge volumes considering temporal changes, whose results could be used as an input for a spatially distributed groundwater-flow model. The present study applies a potential recharge estimation methodology in the SBM, which integrates a combined RS-GIS technique with the analytic hierarchy process (AHP) to assign weights to different hydrologic factors as thematic layers. The proposed methodology is divided into three stages. First, geographic data are collected, processed, and analyzed using GIS and RS tools. Second, long-time-changing factors (assumed static) are used to map the study area's potential recharge (PR) regions. The mapping was done by hierarchizing the spatially distributed data such as geological alignments, drainage network, lithology, surface slope, and historical annual precipitation. In the last stage, the dynamic factors whose data is recorded over the 1970–2019 period of analysis were mapped every 5 years to assess the temporal evolution of potential recharge and its spatial distribution. In this way, the temporal dynamic processes that promote PR are considered by employing a surface water budget equation to estimate PR volumes at each PR region. The novelty of the work is to present a methodology that separates the static parameters to produce a potential recharge zonification from those that vary in time used to calculate the evolution of potential recharge, which facilitates the calibration of the recharge in a groundwater model.

STUDY AREA AND DATA

The SBM covers Mexico City and partially the State of Mexico (Figure 1), with elevations ranging from 2,240 to 5,200 meters above sea level (masl) and an approximate area of 4,080 km². The country's largest and most populated city is located in this area. The city of Mexico hosts more than 22 million inhabitants and generates 22% of the national gross domestic product. A gross volume of 2,142 Mm³/year is required to supply water to the total area's population and 641 Mm³/year for agricultural, industrial, and other service uses (Peña-Díaz 2019). The primary sources of freshwater supply provide the following percentages: 62% comes from the SBM aquifer, 17% from the surface and residual waters, and the remaining 21% is imported from other basins. Currently, the basin is subject to considerable water stress due to the overexploitation of the aquifer.

Data acquisition

Recharge conceptual models are developed using as much input data as is available, and revising and adjusting these models as additional data and analyses provide new insights into the hydrological system. The factors and data that can influence the conceptual model are climate, geology, topography, hydrology, vegetation, and land use. According to Healey & Scanlon (2010), climate variability is often the most critical factor affecting variability in recharge rates. Since precipitation is the source of natural recharge, it is the dominant component in the water budget in most cases. Second, geological aspects such as permeability, soils, and lithologies that can promote recharge must be considered since water quickly infiltrates and drains through the root zone. After that, the surface topography may affect diffuse and local recharge since steep slopes tend to have low infiltration and high runoff rates. Also, hydrology is important because of the natural interaction between surface water and groundwater-flow systems. Not less important is the vegetation and land use since irrigation (for example) may constitute a significant amount of recharge. Lastly, the urbanization component caused by converting natural land to impervious areas that can inhibit recharge must be considered.

The data were collected through public government agencies distributed through official websites and were visualized, analyzed, and pre-processed using 'geographic information systems (GIS)' tools. Table 1 summarizes the collected data and their sources.

METHODOLOGY

The proposed methodology for this work consists mainly of collecting, processing, and analyzing geographic data using GIS tools. This information is handled as layers of thematic information, specifically in shape format (∗.shp), through GIS tools.
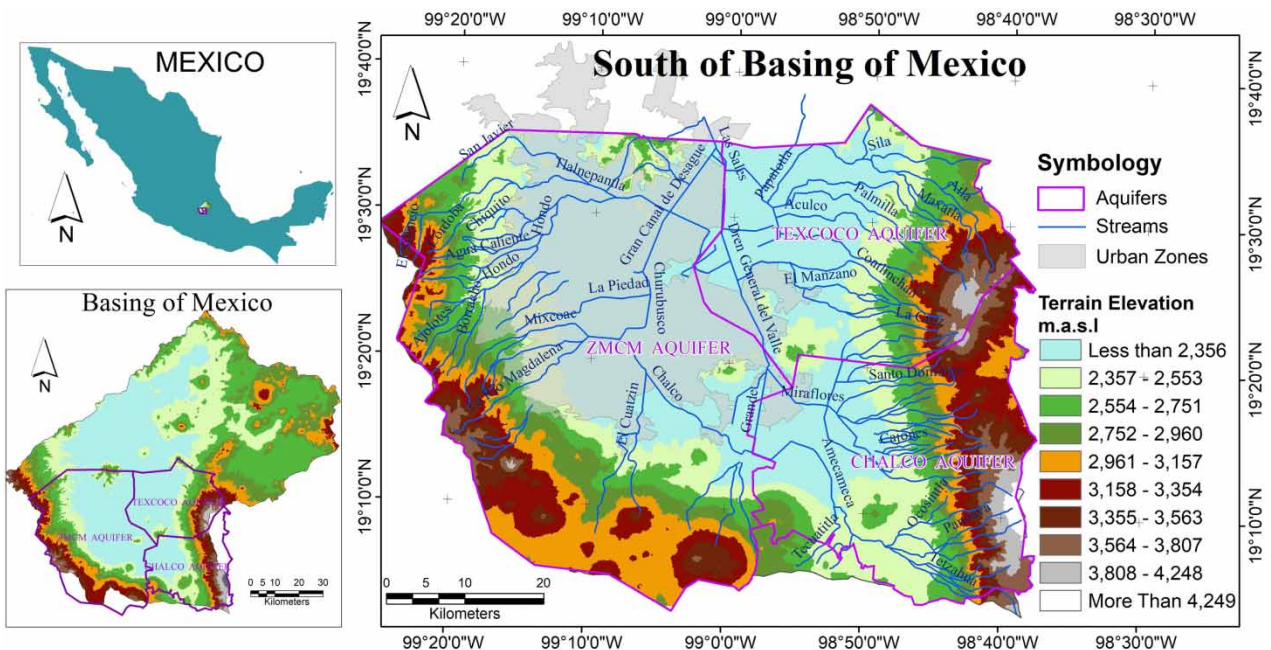

Figure 1 | SBM basin limits, urban zones, administrative aquifers, and main streams.

Table 1 | Main types and sources of information used for this study

| Information	Source	Web link
Cartography (Topography)	INEGI	https://www.inegi.org.mx/
Geology	Mexican Geological Service; Previous Studies (UNAM)	https://www.sgm.gob.mx/GeoInfoMexGobMx/
Geomorphology	CONABIO	http://www.conabio.gob.mx/informacion/gis/
Soil type	INEGI	https://www.inegi.org.mx/
Satellite images	USGS	https://earthexplorer.usgs.gov/
Precipitation	CONAGUA-SMN (CLICOM)	http://clicom-mex.cicese.mx/
Runoff coefficients	US California Waterboards	https://www.waterboards.ca.gov/

This information corresponds to the factors that most influence the potential recharge process in the study area, such as geological alignments, drainage network, lithology, land use, topography, and precipitation. The methodology can be grouped into three stages as follows:

Stage 1. Identification and assignment of weights by zones in each layer of information, according to their physical characteristics favoring recharge.

Stage 2. Regionalization of PR. First, defining weights for each thematic layer using AHP based on importance value. Second, those values are used to apply the 'GIS-weighted overlay' tool to map the PR regions.

Stage 3. Based on the surface water budget equation, a computation for the infiltrated volumes is performed for each PR region. PR regions are areas where groundwater recharge is most likely.

The algorithm in Figure 2 shows the different data and steps followed by the proposed methodology, which accounts for static or long-time-changing factors, and the dynamic or short-time-changing factors in each stage. In the first stage, data of long-time-changing factors such as geological alignments, drainage, topography, lithology, and historic annual precipitation
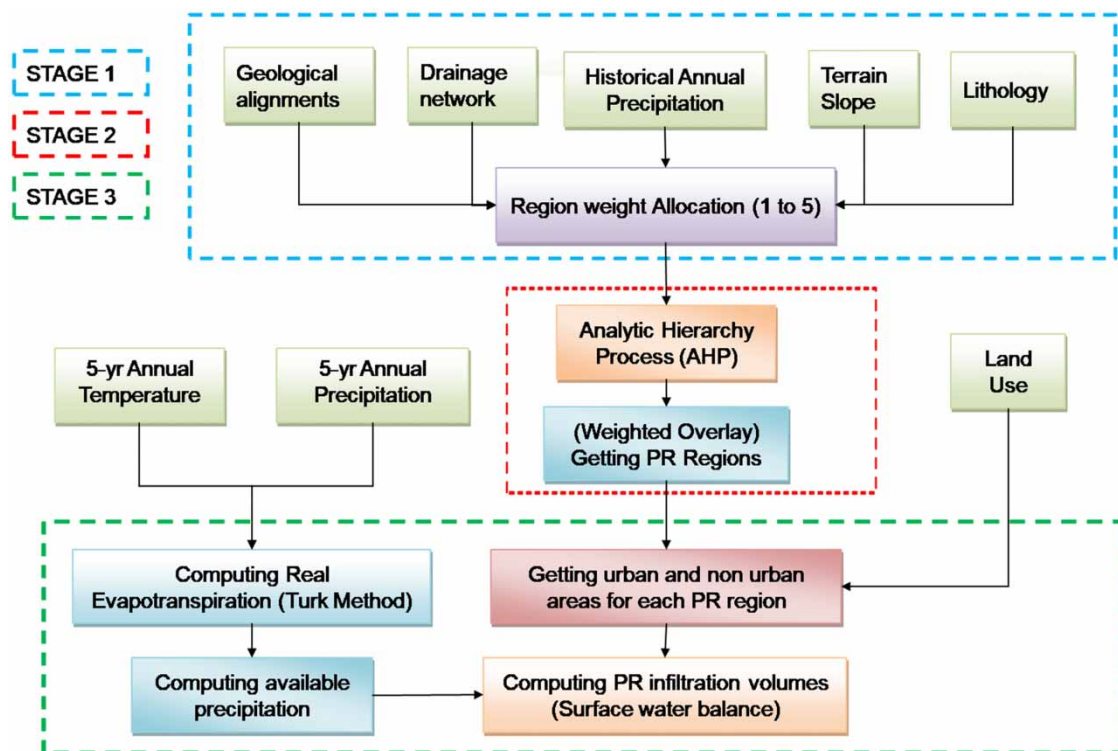
Figure 2 | Methodological procedure to obtain the potential recharge for each PR region.

recorded in a long period (INEGI data from 1920 to 1980) are used for weight allocation and mapped in layer format. Then, in the second stage, each thematic layer is weighted using the AHP methodology, and then, applying the GIS-weighted overlay tool PR regions are mapped. In the third stage, short-time-changing factors recorded from 1970 to 2019 (such as temperature, precipitation, and land use) are used for computing infiltrated volumes at each defined PR region.

The methodology considers spatial heterogeneity by including long-time-changing factors, defining average surfaces for calculating the water budget. These static factors are used to define the PR regions, which are surfaces that allow qualitative analysis of the potential recharge by classifying them into five categories: very poor, poor, moderate, good, and very good. Furthermore, the dynamic factors are subsequently used for the quantitative analysis that comes in phase three, where climate data and land use change are employed to calculate the associated potential recharge amounts for each defined PR region.

Different thematic layers are developed by processing the geographical data described in Table 1. First, a quality analysis of the collected information was carried out before the primary processing. This analysis ensures spatial and temporal precipitation records consistency with the analysis periods over the entire SBM. In addition, anomalies, inconsistencies, missing data, and atypical values were detected by analyzing time series. Consecutively, thematic data layers were mapped within the study area using GIS tools.

Geology is one of the principal factors controlling groundwater's occurrence and movement. The soil texture can be defined as the relative proportion of silt, sand, and clay present in the soil. Clay's smaller pores induce more runoff and less potential recharge, while sandy soils with larger pores induce more potential recharge. Different geological formations can generally be identified according to their lithology and soil type. Also, the terrain slope is crucial because it determines the time required for water to accumulate in each location. The lower the slope, the lower the runoff coefficient, and the higher the potential recharge.

Regarding LUCC, the first refers to 'human activities and various uses that are carried out on the land', while land cover refers to 'vegetation, water bodies, rocks/soil, artificial cover and others resulting due to transformations'. LUCC defines the potential recharge rate of rain and water. On the other hand, drainage density depends on the slope, the nature, and attribute of the parent rock, and the regional and local fracture patterns. The drainage network reflects the lithology and structure of a particular area and is studied according to two parameters: (a) drainage pattern, associated with the nature and structure of the substrate and (b) the drainage texture, which is related to the permeability of the rock/soil. The less permeable rock, the lesser potential recharge, and minor weights are assigned to those areas. While geological alignments are linear or curvilinear structures on the Earth's surface and represent the weakest zone of the bedrock. Also, alignments may be correlated with faults, fractures, joints, bedding plans, and lithological contacts.

Essential components of the short-time-changing factors are precipitation and temperature since a proportion of the total precipitation volume infiltrates, but the rest is removed by runoff or evapotranspiration processes. In the area, 132 climatic stations are present, but following the criteria proposed by Salas et al. (1980) and Sánchez-Quispe et al. (2021), only 85 were used to interpolate the precipitation and temperature raster files for the established periods of analysis, generated as the average of 5 years, between 1970 and 2019. Next, Table 2 describes the procedure to generate each thematic layer. Thematic maps such as geology, terrain slope, land use and land change, drainage network, and alignment density were generated using satellite images and conventional data to assess PR regions.

Calculation of PR volumes

Groundwater models (GWMs) can assess changes from hours or days to seasons or years (transient conditions), and are typically used to assess changes in the steady-state water balance. However, groundwater monitoring data is generally scarce and is taken as representative of the long-term average condition (steady state). In this study, the estimation of the aquifer potential recharge is carried out at a 5-year interval from 1970 to 2019 following a methodology based on the surface water budget equation. According to Gómez-Reyes (2013), the water budget equation should be the precipitation volume (P) equal to the sum of the outputs represented by runoff (R), evapotranspiration (ET), and infiltrated volume or PR. Solving for the potential recharge, the water budget equation (Equation (1)) can be written as follows:

$$PR = P - (ET + R) \tag{1}$$

The equation is then multiplied by the basin area (Ba) to get the result in volume units. In this case, both terms ET and R are the system's outputs. The direct runoff of the basin depends on the LUCC and can be calculated using the rational formula as

Table 2 | Data processing description for each layer

Layer	Generation process description
Geology	It was generated from the collected map using GIS tools. Different classes of lithology were identified and assigned weights, according to their relative importance in groundwater occurrence or recharge.
Terrain slope	The slope map is prepared from the digital elevation model (DEM) and then divided into different classes. Appropriate weights (1–5) were assigned to each class, based on their contribution to groundwater occurrence.
Land use/land cover	Satellite imagery (NASA Landsat imagery) was used to classify and produce a LUCC thematic layer; thus, the urban and non-urban land type areas were associated with the respective runoff coefficients (Table 3).
Drainage density	The drainage lines are digitized from the rectified remote sensing images for the study area and verified with thematic mapping. Drainage density is then computed by dividing the cumulative length of all streams by the total area. Regions with high density will have a lower weight, due to the runoff does not favor water retention for potential recharge.
Geological alignments	The alignments were identified through satellite images and their density was obtained similarly to the drainage network, applying a similar equation to obtain the density of alignments per unit area.
Precipitation and temperature	Average data for annual precipitation and temperature were obtained from the CLICOM (2021) database, extracting historical records for each related climatic station (Figure 1). Consistency tests were performed on the precipitation series so that they meet the conditions of randomness, homogeneity, independence, and seasonality (Merlos-Villegas et al. 2014; Sánchez-Quispe et al. 2021).

$R = Ce*Pa*Ba$, where Ce is an equivalent runoff coefficient, and Pa is the available precipitation (calculated as P – ETR). Runoff coefficient is the less accurate component since it implies a relation between discharged peak runoff and precipitation rates (varies from 0 to 1). Appropriate runoff coefficient selection is based on knowledge of specific characteristics of the study area. In this way, runoff depends on permeability, surface slope, and flood characteristics. Impermeable surfaces such as pavement or roofs will produce a runoff coefficient close to 1 regardless of the surface slope. In general, the runoff coefficient depends on the nature of the surface, surface slope, and rainfall intensity, while its selection must be carefully performed to include all those factors. For the urban areas, the value of Ce = 0.60 from SACMEX (2005) was adopted since it considers the possible variations due to housing developments, roads, sidewalks, and the so-called green areas. While for heterogeneous surfaces, an equivalent runoff coefficient is computed using Equation (2), to include all non-urban areas for the different PR zones. Table 3 shows some selected runoff coefficients (Ci) for the study zone, based on the California Waterboards (2011).

$$Ce = \frac{\sum_1^n Ci}{A} \tag{2}$$

Table 3 | Selected runoff coefficients Ci for non-urban areas

Land use	Selected Ci	Range	Description
Bare soil	0.30	0.2–0.5	Rough
Urban	0.60	0.4–0.75	Residential
Agricultural (with crop)	0.35	0.2–0.5	Heavy soil
Agricultural (no crop)	0.45	0.3–0.6	Heavy soil
Unimproved areas	0.20	0.1–0.3	Bushes, weed
Pasture	0.15	0.05–0.25	Sandy soil
Woodlands	0.25	0.05–0.25	Slope > 6%
Wetlands	0.01	0.01–0.05	Silty soil

The ET term is replaced with the real evapotranspiration (ETR), calculated with the Turc equation (Equation (3)). This method uses the precipitation (P) and temperature (T) patterns, representative of each PR region, through the following expression:

$$\text{ETR} = \frac{P}{\sqrt{0.9 + \left(\frac{P^2}{L^2}\right)}} \qquad (3)$$

where ETR is in mm/year, P is the mean precipitation per 5-year period, in mm/year, $L = 300 + 25\,t + 0.05\,t^3$, with t as the mean annual temperature for periods of 5 years, in degrees Celsius.

Potential recharge volumes are calculated using mapped PR regions and the corresponding land use areas within each surface. First, the total volume of water capable of generating surface runoff is computed by multiplying the available precipitation layer by its corresponding overlapping PR region. Secondly, infiltrated water volume in each PR region is estimated by subtracting the previously computed runoff volumes from the total volume. The water budget equation can be written as Equation (4) and applied to calculate the volume of potential recharge:

$$\text{Vi} = \text{Vt} - [(\text{Pa} * 0.6 * \text{Au}) + (\text{Pa} * \text{Ce} * \text{An})] \qquad (4)$$

where Vi is the average volume infiltrated for a 5-year period, Vt is the total precipitation volume of each PR region, Pa is the available precipitation, Au is the urban surface, and An is all other non-urban surfaces.

Like any other balance, the water budget proposed here is only a basic tool that can be used to assess the occurrence and movement of water in the natural environment. Average state conditions are generally analyzed, and the representing equation can be very simple or complex, depending on the studied environment and its objectives. The water budget analysis would provide an initial understanding of the system that can be later refined as more data becomes available. As a complement, a numerical model would provide a more refined understanding of the subsurface and surface flow system, at different scales and levels. Nevertheless, it is also important to recognize uncertainty in all water budget components associated with the natural variability of the hydrological cycle and measurement errors (Healy *et al.* 2007).

Analytic hierarchy process

The AHP is a simple tool to help decision-makers; it is used in decision-making problems that involve very complex processes. It was developed in the late 1960s by Saaty (1990), who based his research on the military field and his teaching experience. In this way, the AHP allows discerning between different processes to determine a solution that best satisfies the combination of possible alternatives (Osorio & Orejuela 2008). The first uses of the AHP were given to solve decision problems in multicriteria environments.

The priorities of the elements in each level are defined by assigning a specific weight, and then they are added to obtain the total weight of global priorities. These total weights, compared against the alternatives, become an important support element for decision-making. The total weight of the alternative W_j (Equation (5)) is determined for all objectives, such as:

$$W_j = w_{1j}w_1 + w_{2j}w_2 + \cdots + w_{mj}w_m \qquad (5)$$

where, for i given targets ($i = 1, 2, \ldots, m$), the respective weights w_i are determined, and for each target i, the $j = 1, 2, \ldots, n$ alternatives are compared and the weights w_{ij} are determined. The alternatives are ordered according to the W_j in descending order, where the highest value indicates the most preferred alternative.

Goepel (2013; 2018) implements the method based on the solution of an eigenvalue problem. This way the results of the pairwise comparisons are arranged in a matrix. The matrix's first (dominant) normalized right eigenvector gives the ratio scale (weighting), and the eigenvalue determines the consistency ratio (CR). The process follows the next steps: (1) get pairwise comparisons of the factors; (2) apply selected AHP judgment scale; (3) fill the decision matrix from pairwise comparisons; (4) find the eigenvector using the power method; (5) calculate the dominant eigenvalue from the eigenvector; (6) calculate the consistency ratio (CR); (7) calculate the inconsistency matrix; (8) identify and highlight the top three inconsistencies; and (9) go back to step 1 until the user submits his judgments.

According to Goepel (2013; 2018), the AHP process is performed by filling out questionnaires which may require further clarifications about the completion procedure or pairwise comparison. In this way, AHP hierarchies are derived from the most consistent matrices. A measure of consistency is the consistency index (CI). From this, a consistency ratio $CR = CI/RI$ is derived, using a randomized index (RI), the average CI for randomly filled matrices. Also, a parameter α is needed as a level of consistency to adapt the cut-off value ($CR < \alpha$), for declaring the matrix inconsistent. Saaty's rule of thumb is to accept only judgment matrices with $CR < 0.1$.

A consensus measurement that includes an aggregated group of results is calculated for a group decision-making factor is calculated based on Goepel (2018). This process includes Shannon entropy in two independent components (alpha and beta diversity) to derive the AHP consensus indicator. The similarity measure S (or consensus indicator) depends on the number of criteria and uses a linear transformation to map it to a range from 0% (no consensus) to 100% (full consensus). This range is then categorized into five categories: very low (<50%), low (50–65%), moderate (65–75%), high (75–85%), and very high (>85%).

RESULTS AND DISCUSSION

Stage 1

Historic annual precipitation

In this stage, long-time-changing parameters, such as the annual precipitation map, are used for weighting. This data was retrieved from the INEGI database (Table 1) and covered a longer period than the one analyzed (1970–2019). The data were compared with that for the analyzed period, and no significant differences were observed in the precipitation pattern between both data sources. The aquifer is recharged mainly by precipitation, while surrounding mountains act as the most important natural recharge areas (Figure 3(a) and 3(b)). The average annual precipitation ranges from 600 to 720 mm in the lower part of the study area. In contrast, in the surrounding hills, the average annual precipitation ranges between 730 and 1,100 mm, and in the mountains within the limits of the basin, the precipitation may surpass 1,200 mm/year.

Lithology

Lithology and edaphology are other long-time-changing parameters that are basic to calculate recharge volumes. The geological–lithological data (Figure 4(a) and 4(b) and Table 4) were taken from Arce *et al.* (2019) who identified the principal formations, according to the materials' geological ages. Hierarchical zones were established according to their potential recharge capacity in each lithological unit by considering their characteristics. The Sierra Nevada is characterized by strato-volcanoes range such as Monte Tláloc, Telapón, Iztacihuatl, and Popocatepetl, constituted of andesitic, dacitic, and slightly rhyolitic composition. Ages range from 1.2 Myr to the present. Another mountain range is the Sierra de las Cruces, comprised of intermingled domes and volcanoes with associated pyroclastic deposits. The chemical composition varies from andesite to
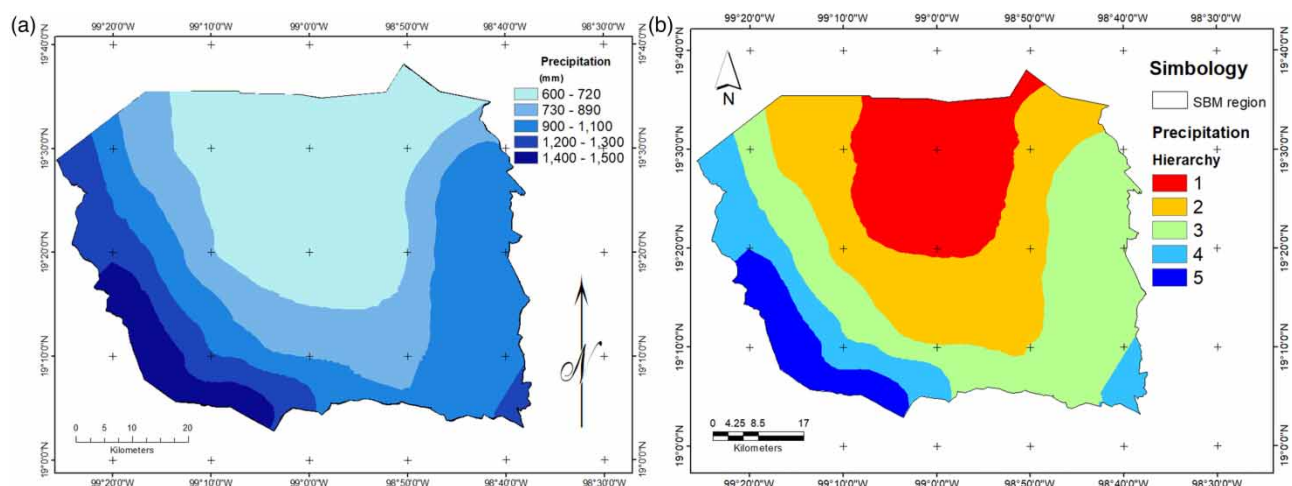

Figure 3 | (a) Mean annual precipitation. (b) Spatial reclassification of precipitation by five hierarchical areas.
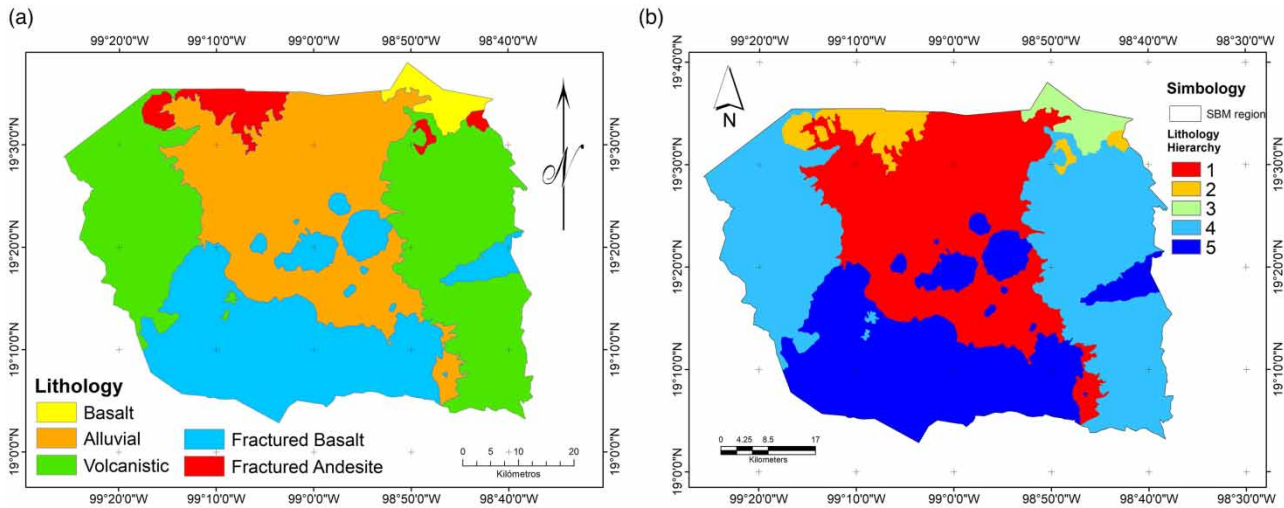
Figure 4 | (a) Geology (Source: Arce et al. 2019). (b) Hierarchy of geological units.

Table 4 | Analyzed lithological criteria for weight determination

Lithological formation	Description
Apan	Tuffs in Piedmont, intermediate vulcanites.
Chichinautzin	Fractured volcanic rocks, fluid structures with regular loosening and phenocrysts of labradorite, olivine, hypersthene, and augite; phenobasalts or andesites (dacitic–rhyolitic rocks); cones and domes, deposits of tezontle and ash from the 'Sierra de Santa Catarina'.
Tepoztlan Formation	Vulcanites and pyroclastic flows of the Tepozteco Formation.
Lacustrine	Alluvial sediments, clays, tephras, and 300 m thick sediments.

dacite, with ages ranging from 3.7 to 0.4 Myr. Another important geological formation is the Chichinautzin volcanic field, formed by more than 220 monogenetic volcanoes of heterogeneous composition (from basalt to dacite), where the ages range from 1.2 Myr to 1.6 kyrs. Also, the valley is occupied by up to a 300 m thick layer of lacustrine deposits of sediments interlaced with volcanic tephras, with ages of 220 kyrs to the present.

Geological alignments

The alignments were obtained from satellite images using automated extraction techniques that increase the details of existing data and available geological structures. The main advantages of automatic lineament extraction are their ability to process uniformly using different images (processing operations are performed quickly) and their ability to extract alignments not recognized by the human eye. In this study, the LINE module of PCI Geomatica 9.1 software performed the automated extraction of lineaments using Landsat images downloaded from the USGS. Figure 5(a) shows the resulting alignment map. The lineament density map 5(b) was generated using the 'ArcGIS Spatial Analyst Tool'. The linear density values were then ranked on a scale from 1 to 5 (Figure 5(b)).

Terrain slope

Figure 6(a) shows the different terrain slopes in percentage, from smooth slope (red-colored) to steep slope (dark-blue-colored). In general, flat and smooth slopes promote potential recharge and groundwater recharge, and conversely, steep slopes promote runoff and little or no potential recharge. Therefore, considering the slope the flattest areas (blue areas in Figure 6(b)) are the most likely to promote potential recharge.
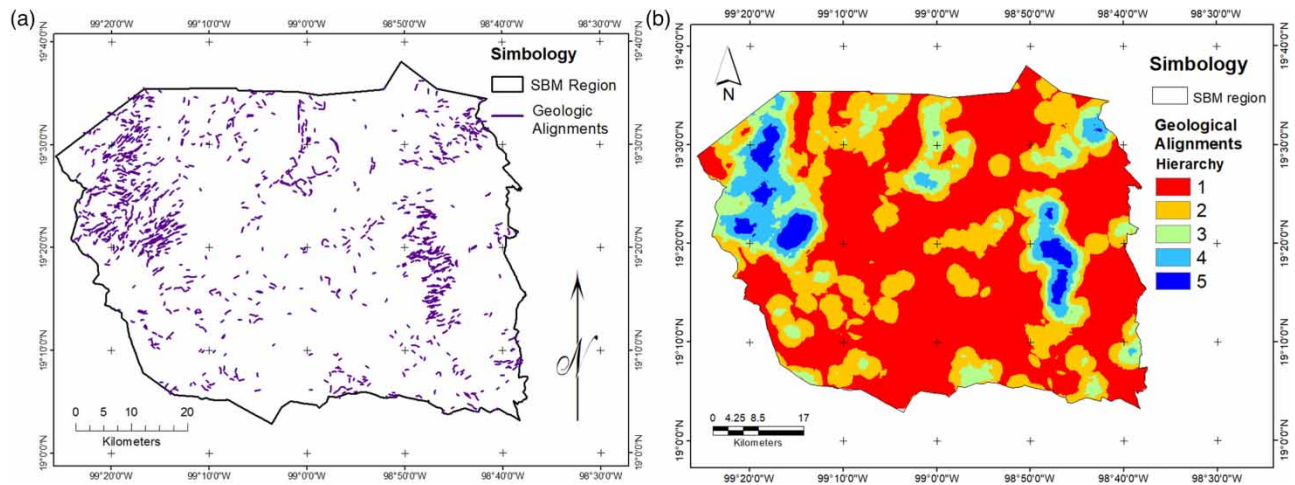
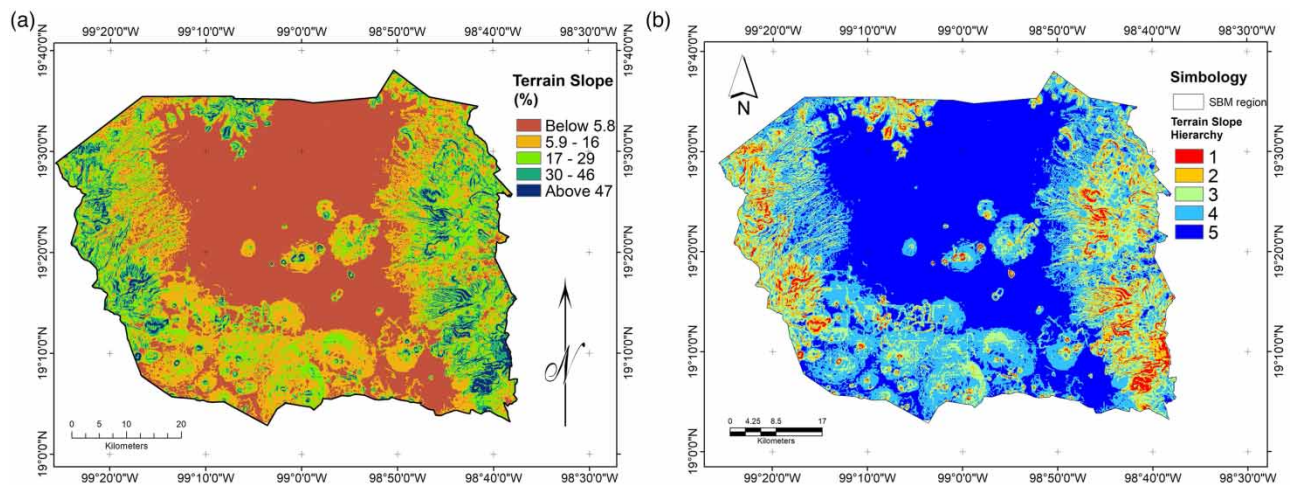**Figure 5** | (a) SBM geologic alignments. (b) SBM alignment density hierarchy.

Figure 6 | (a) The slope of the land in percentage (Source: INEGI). (b) Hierarchy of % slope from 1 to 5. Please refer to the online version of this paper to see this figure in colour: https://dx.doi.org/10.2166/nh.2023.103.

Drainage network

Initially, natural channels flowed through the Valley of Mexico and filled an ancient lake system, which nowadays has been drained and covered by urban areas. The natural river network has been transformed into the city's drainage and sewage system. The ancient lake system was purposely dried to allow urban development by piping runoffs outside of the SBM. Now, natural channels are found in the mountainous area of the basin, mainly in the Sierra Nevada and Las Cruces. The Chichinautzin formation presents lower surface runoffs (Figure 7(a)) and greater potential recharge.

The drainage pattern is one of the most important indicators of the potential recharge process because the underlying lithology mainly controls drainage patterns and density. Furthermore, the stream pattern reflects the potential recharge rate of precipitation compared with surface runoff. The potential recharge/runoff rate is mainly controlled by permeability, which is a function of rock type and the underlying bedrock fractures. Comparing mountainous terrains and valleys, the one with the higher drainage density is usually less permeable. Therefore, the denser the drainage network, the lower the recharge, and vice versa. Figure 7(a) and 7(b) shows the resulting density mapped with the spatial analyst GIS software, ranked from 1 to 5.
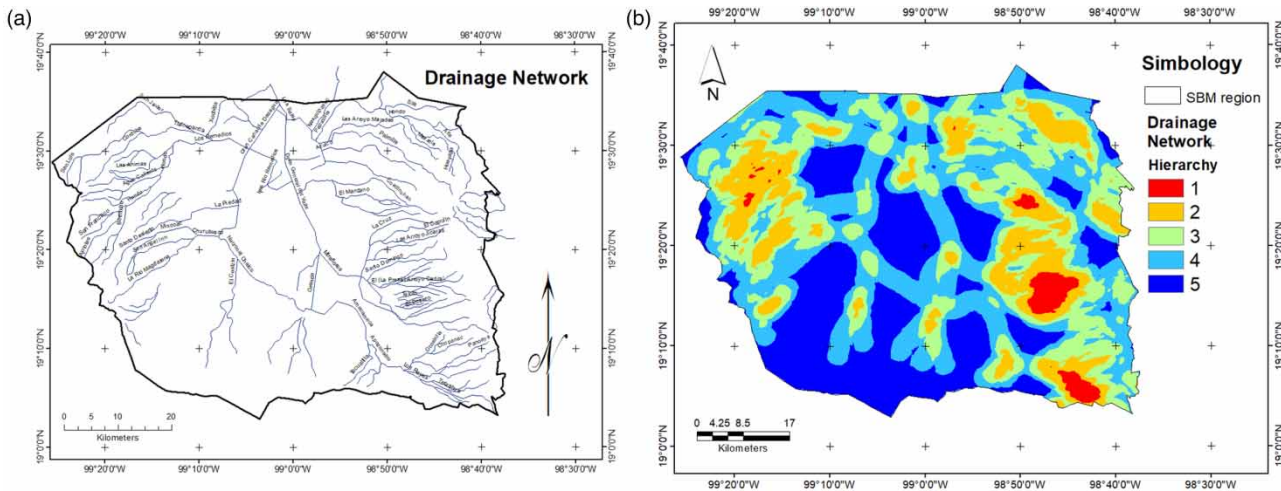
Figure 7 | (a) SBM drainage network (Source: INEGI). (b) Drainage density ranging from 1 to 5.

Results Stage 2

Layer weighting using AHP

To map the highest and lowest PR regions, the 'GIS-*weighted overlay tool*' was used. This tool requires analysis layers to be supplied with a certain percentage of influence. This influence was computed using the AHP technique to structure, measure, and synthesize information. In this case, to assign a specific weight, layer importance and hierarchy of the proposed thematic GIS layers were considered. The methodology was applied as in Goepel (2018) using an online AHP calculator. First, ten pairwise comparisons were performed for the five factors using a questionnaire. The answers should include the importance on a scale of 1–9. AHP Scale: 1 – Equal importance, 3 – Moderate importance, 5 – Strong importance, 7 – Very strong importance, and 9 – Extreme importance. The questionnaire answers are highlighted in Table 5; this was done using experience and knowledge of the study area. The consistency ratio was CR = 6.3%, considered satisfactory (<10%).

The hierarchies of each factor are the resulting weights from the pairwise comparisons. Those weights are assigned to each layer based on the principal eigenvector of the decision matrix. In this case, the principal eigenvalue was 5.28, with 6 iterations and $\delta = 3.1^{-9}$. Table 6 summarizes the resulting factor hierarchy ranks and priority percentages. Those were used as input to the GIS-weighted overlay tool.

Table 5 | Factors pairwise comparisons questionnaire, with highlighted answers

	Chose Priority		Equal	How much more?								
n	A	B										
1	Precipitation	Lithology	1	2	3	4	5	6	7	8	9	
2	Precipitation	Alignments	1	2	3	4	5	6	7	8	9	
3	Precipitation	Slope	1	2	3	4	5	6	7	8	9	
4	Precipitation	Drainage	1	2	3	4	5	6	7	8	9	
5	Lithology	Alignments	1	2	3	4	5	6	7	8	9	
6	Lithology	Slope	1	2	3	4	5	6	7	8	9	
7	Lithology	Drainage	1	2	3	4	5	6	7	8	9	
8	Alignments	Slope	1	2	3	4	5	6	7	8	9	
9	Alignments	Drainage	1	2	3	4	5	6	7	8	9	
10	Slope	Drainage	1	2	3	4	5	6	7	8	9	

Table 6 | AHP factor hierarchy ranks and priority percentages results

Factors		Priority	Rank	(+)	(−)
1	Precipitation	51.6%	1	20.0%	20.0%
2	Lithology	25.9%	2	10.2%	10.2%
3	Alignments	15.0%	3	6.4%	6.4%
4	Slope	4.1%	4	1.1%	1.1%
5	Drainage	3.5%	5	1.2%	1.2%

Delimitation of PR regions

In the present study, PR regions are delineated using GIS techniques. First, thematic layers of long-time-changing factors were included: geology, drainage density, annual precipitation, and geologic alignments. Each layer is a thematic map of regionalized weights (from 1 through 5, where the higher the number, the better PR); after that, total layer weights were assigned to each one using the AHP technique. Then, the 'GIS-weighted overlay tool PR regions' were mapped. The PR regions for this work were defined into five categories: very poor, poor, moderate, good, and very good.

The GIS-'spatial analyst-weighted overlay' tool uses the weights generated in the AHP method to obtain the PR regions. The resulting map in Figure 8 shows that while the surrounding mountain ranges are good and very good potential recharge regions (light and dark green areas), the urban area's surface corresponds to the regions of poor and very poor potential (orange and red areas).

The mapped PR regions reflect long-time-changing parameters that are fixed for the rest of the analyses. Notably, the largest PR regions correspond to poor and moderate (orange and yellow areas), with 33.9 and 37.5% of the SBM total area (4,080 km²), respectively. These two areas, together with the very poor PR with just 0.1%, represent the lowest percentage of recharge for all regions; in turn, they present the highest percentage of the urbanized surface along the analyzed 5-year periods. On the other hand, the good and very good PR regions, with 24 and 4% of the SBM surface, respectively, presented the smallest urbanized areas along the periods. These percentages concord with what was found by Boyás Martínez *et al.* (2021), whose results showed that the medium category predominates over the entire area. However, they also include two additional aquifers in the northern part of the Basin of Mexico. On the other hand, in their study, the good and very good areas represented 19.1 and 5.2% of the SBM total area, respectively, values slightly smaller than the ones reported in this work.

Results Stage 3

Calculation of potential recharge volumes

LUCC and the other equation parameters for the surface water budget were generated for the 1970–2019 period in raster format for subperiods of 5 years. For LUCC data, satellite images were used, one as representative for each period: 1970–1974, 1975–1979, 1980–1984, 1985–1989, 1990–1994, 1995–1999, 2000–2004, 2005–2009, 2010–2014, and 2015–2019, to determine the change due to urbanization and deforestation over time. The SBM aquifer recharge zone has been previously identified at the south and southwest of the urban area and the external supply areas in the State of Mexico. Those areas are threatened by the growth of urban expansion, triggering different environmental problems, such as the loss of ecosystems and conservation lands. Previous works have calculated, on average, 2.5 million liters of water loss per year for every hectare that is urbanized. Excessive urbanization is a consequence of irregular settlements on conservation land, with about 26.93 km², stopping potential recharge by approximately 6,734 million liters of water per year, equivalent to the annual supply of more than 70,000 people (PAOT 2009). Figure 9 shows classified images for some selected periods, where dark colors represent urbanized regions, green colors forested regions, and reddish and yellow represent agricultural regions. The rest of the classifications are found in the Supplementary material.

Urban and non-urban areas were remotely detected for the study area developing LUCC layers through Landsat images downloaded from the USGS agency's EarthView website. The images were classified using the free Multispec® software (Biehl & Landgrebe 2002). Table 7 shows the classified image representative of each 5-year between the years 1970 and 2019.

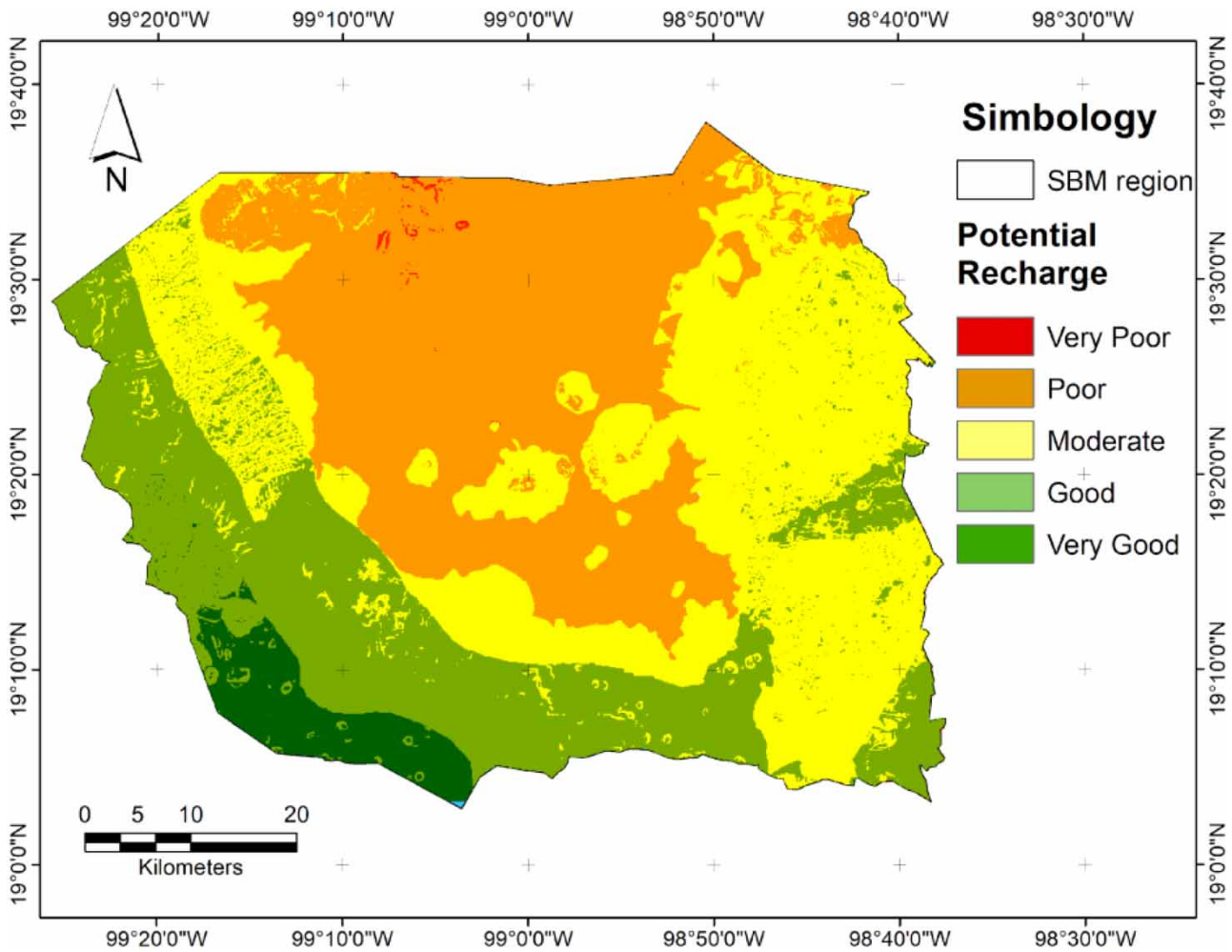**Figure 8** | PR regions included within the SBM region. Please refer to the online version of this paper to see this figure in colour: https://dx.doi.org/10.2166/nh.2023.103.

The 5-year LUCC layers and the PR regions map (Figures 8 and 9) were used to obtain the proportions of urban and non-urban areas. Urban areas include housing developments, roads, sidewalks, and parks, while non-urban areas include bare soil, agricultural land pasture, woodlands, and wetlands. The respective runoff coefficients were selected for each land cover (Table 3), including soil properties and surface slope. A global runoff coefficient for each PR region was computed as an equivalent runoff coefficient (Ce). Table 8 shows the respective computed values of Ce for each of the analyzed 5-year periods by PR regions in the study area.

Average annual temperature

The average temperature, as the precipitation data, was extracted for the 1970–2019 period in raster format for periods of 5 years: 1970–1974, 1975–1979, 1980–1984, 1985–1989, 1990–1994, 1995–1999, 2000–2004, 2005–2009, 2010–2014, and 2015–2019. Figure 10 shows the kriging interpolation generated for annual temperature for four selected periods between 1970 and 2019 (the rest are found in the Supplementary material). Discrete values correspond to 1×1 km square pixels, representing the interpolated data. It can be seen that the warmest areas with temperatures of 14.8–17.7 °C (dark orange to red colors) are found in the valley region and coincide with the most urbanized area. On the other hand, the coolest surfaces of 9.3–14.8 °C correspond to the slopes of the mountains and the ranges (light orange to yellow colors). This data was used to calculate the real evapotranspiration (ETR) using the Turc method (Equation (3)).
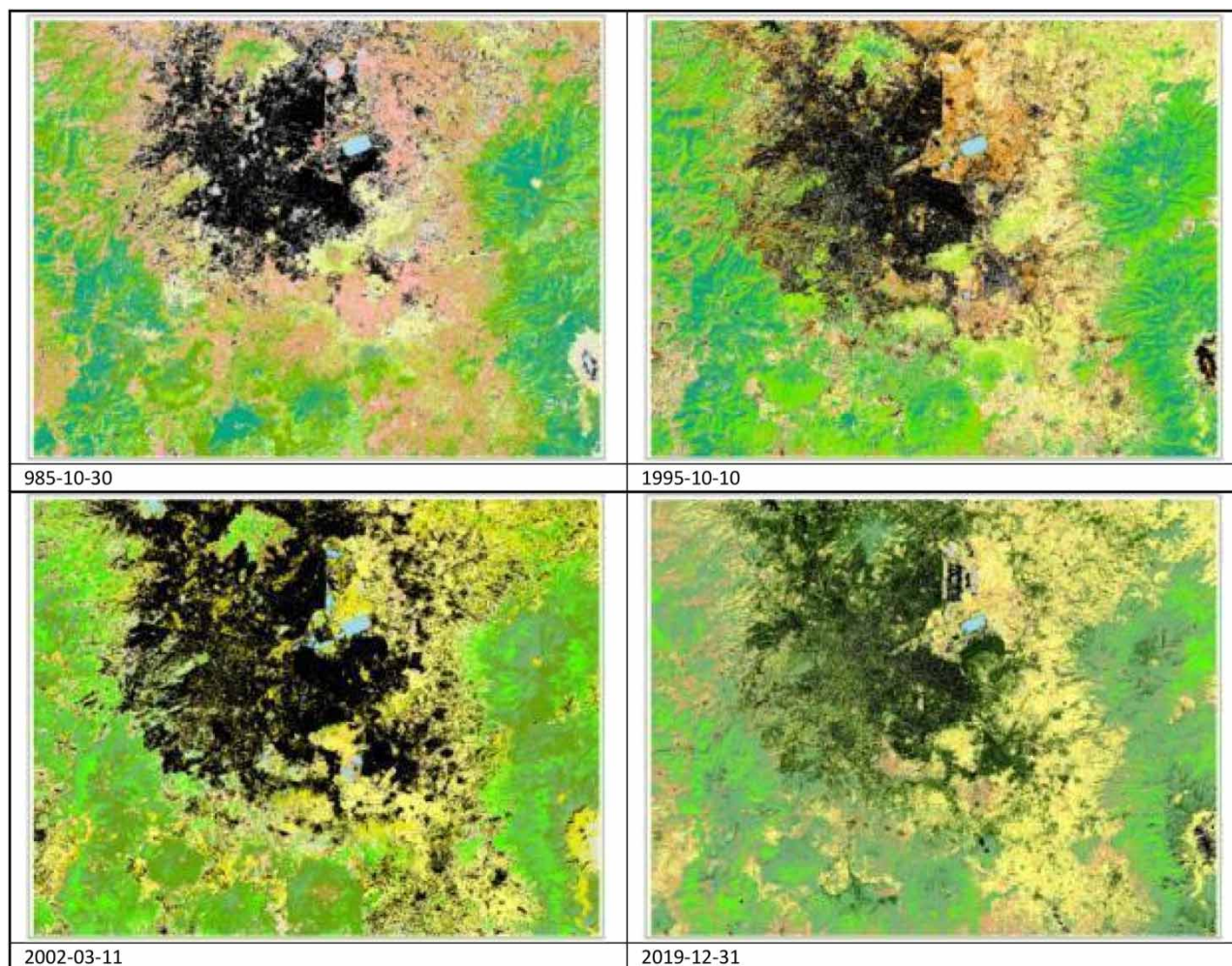
Figure 9 | Classified images for selected time periods. Please refer to the online version of this paper to see this figure in colour: https://dx.doi.org/10.2166/nh.2023.103.

Average annual precipitation

The same as temperature, precipitation records were analyzed for 1970–2019 at 5-year intervals. First, raw precipitation records were obtained from the CLICOM (2021) database for the analysis period. Figure 11 shows that average annual precipitation for four of the selected periods (the rest are found in the Supplementary material), where isolines follow a pattern like that observed in the average annual temperature but, in this case, the lowest precipitation value (501.9–798.3 mm) occurs in urban areas of the valley, while in mountainous regions, the values range from 798.3 to 1470.9 mm. This data was also used to calculate the actual evapotranspiration (ETR) using the Turc method (Equation (3)), which is subtracted from the total precipitation to estimate the available precipitation (Figures 12(a) and 12(b)).

Potential recharge volumes were calculated using the surface water budget (Equation (4)) for the 1970–2019 period and for each 5-year time interval using data in raster format with the GIS-Map Algebra tool. Then, the potential recharge volumes were computed using Equation (4) for each PR region with the different urban and non-urban land use areas, through their respective associated runoff coefficients Ce. Afterward, ETR was calculated for the representative or average records of each PR region (Figure 12(b)). A map of the available precipitation layer is shown in Figure 12(a), used to generate the surface runoff and potential recharge, by subtracting the calculated value of the ETR from the total precipitation for each period of analysis. As an illustration, Figures 12(a) and 12(b) show the resulting maps of real evapotranspiration and available precipitation for selected periods, while the rest are found in the Supplementary material.

Table 7 | Characteristics of Landsat satellite images used

Representative period	Landsat product ID	Spacecraft ID	Sensor ID	Date acquired	Grid cell size (m)		
					Reflective	Thermal	Panchromatic
1970–1974	'LM02_L1TP_028047_19 760327_20180424_01_T2'	'LANDSAT_2'	'MSS'	27 March 1976	60		
1975–1979	'LM03_L1GS_028046_19 791110_20200906_02_T2'	'LANDSAT_3'	'MSS'	10 November 1979	60		
1980–1984	'LM05_L1TP_026047_19 851030_20180407_01_T2'	'LANDSAT_5'	'MSS'	30 October 1985	60		
1985–1989	'LT05_L1TP_026047_199 00318_20170131_01_T1'	'LANDSAT_5'	'TM'	18 March 1990	30	30	
1990–1994	'LT05_L1TP_026047_199 51010_20170107_01_T1'	'LANDSAT_5'	'TM'	10 October 1995	30	30	
1995–1999	'LT05_L1TP_026047_200 01210_20161213_01_T1'	'LANDSAT_5'	'TM'	10 December 2000	30	30	
2000–2004	'LE07_L1TP_026047_200 20311_20170131_01_T1'	'LANDSAT_7'	'ETM'	11 March 2002	30	30	15
2005–2009	'LT05_L1TP_026047_201 00205_20161017_01_T1'	'LANDSAT_5'	'TM'	5 February 2010	30	30	
2010–2014	'LC08_L1TP_026047_201 50713_20170226_01_T1'	'LANDSAT_8'	'OLI_TIRS'	13 July 2015	30	30	15
2015–2019	'LC08_L1TP_026047_201 91231_20200111_01_T1'	'LANDSAT_8'	'OLI_TIRS'	31 December 2019	30	30	15

Table 8 | Estimated Ce values for each PR region and each 5-year period over the SBM

PR region	1970–1974	1975–1979	1980–1984	1985–1989	1990–1994	1995–1999	2000–2004	2005–2009	2010–2014	2015–2019
Very poor	0.34	0.32	0.31	0.33	0.26	0.33	0.40	0.40	0.38	0.31
Poor	0.32	0.31	0.30	0.31	0.25	0.29	0.31	0.40	0.31	0.31
Moderate	0.31	0.27	0.26	0.28	0.24	0.26	0.29	0.32	0.28	0.29
Good	0.28	0.26	0.25	0.26	0.23	0.25	0.27	0.29	0.26	0.27
Very good	0.23	0.25	0.25	0.24	0.22	0.25	0.24	0.28	0.24	0.26

Figure 13 shows the potential recharge in millimeters for each classified PR region for each 5-year interval. In the very poor and poor regions comprising the most urban areas, the proportion of potential recharge from rainfall was the lowest, with an average of 13% for both. This amount makes sense since the very poor area is tiny; besides, this is closer to the value reported by Son & Kwon (2022) for urban parks. While in the moderate PR region, 20.4% of precipitation is infiltrated. This value is higher than the one Ruiz (2015) reported for plain areas; however, their study area was shorter and only considered part of the mountainous region where precipitation is highest in the study area. Furthermore, the highest values of potential recharge correspond to good and very good areas, with 30 and 41%, respectively. Also, the obtained very good PR region is lower in surface extent than the moderate PR region (Table 9), where an extended surface may compensate for lack of potential recharge. The assessed values of good and very good PR regions fall in the precipitation potential recharge range obtained by Ortega & Farvolden (1989), with 30–50% in mountain areas, although their study was done using hydrological sections.

The graph shown in Figure 14 summarizes the results, revealing a cyclical pattern in the annual precipitation, while the recharge has similar but less pronounced behavior. On the other hand, the urbanized area (blue line) and the potential recharge volume (purple line), both in percentage, reveal a decreasing trend during each period; the increase in urbanization may cause it. The results show that periods with greater slope in the percentage of potential recharge coincide with a greater
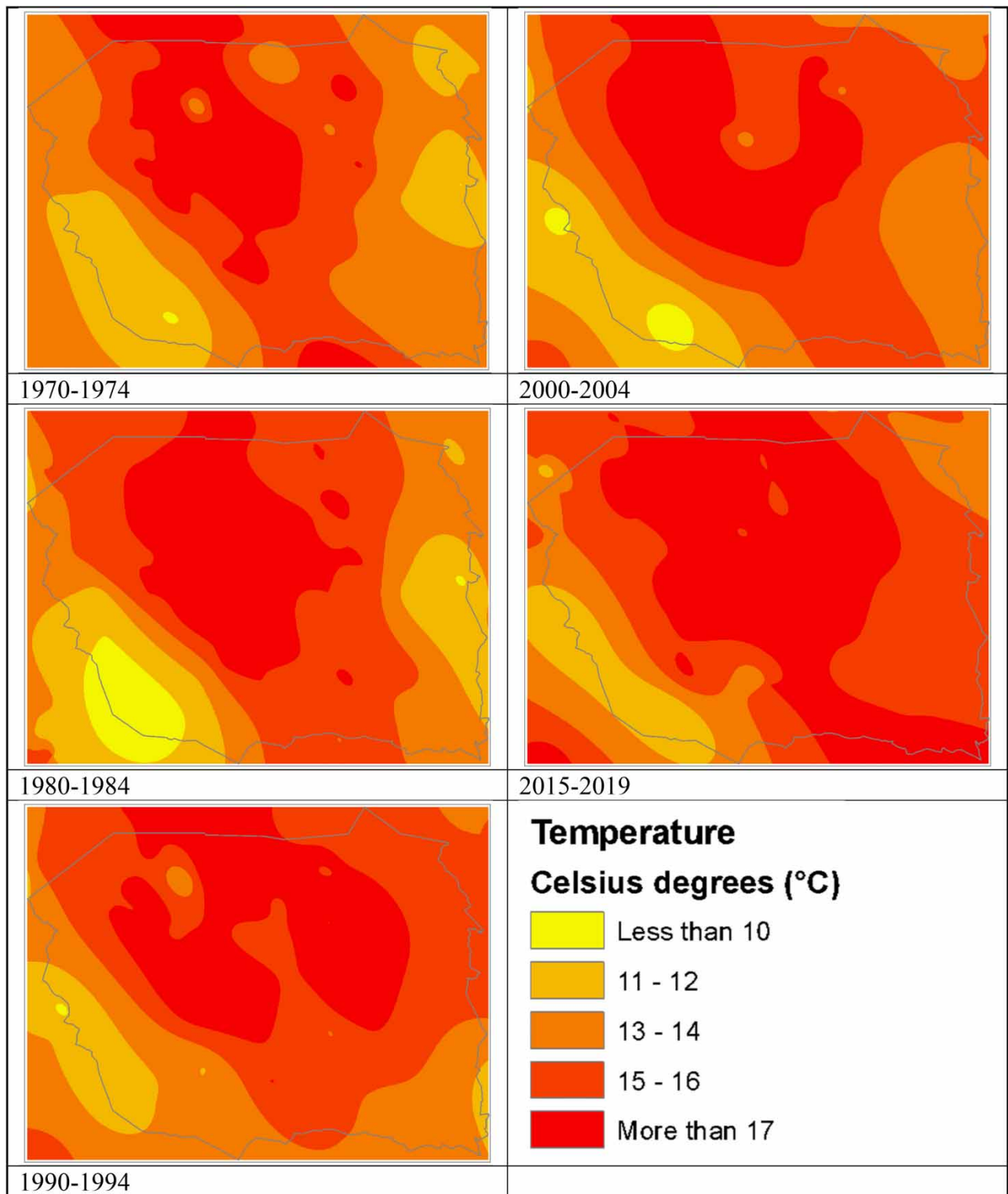
Figure 10 | Average annual temperature for four of the selected 5-year periods. Please refer to the online version of this paper to see this figure in colour: https://dx.doi.org/10.2166/nh.2023.103.

increase in urbanization. This may suggest an inverse proportionality of urbanization with potential recharge. In the 1980–1989 period and, more recently, the 2010–2019 period, the decrease in potential recharge and the increase in urbanization make both variables almost mirror each other. In some portions of the graph, a slight increase in potential recharge is
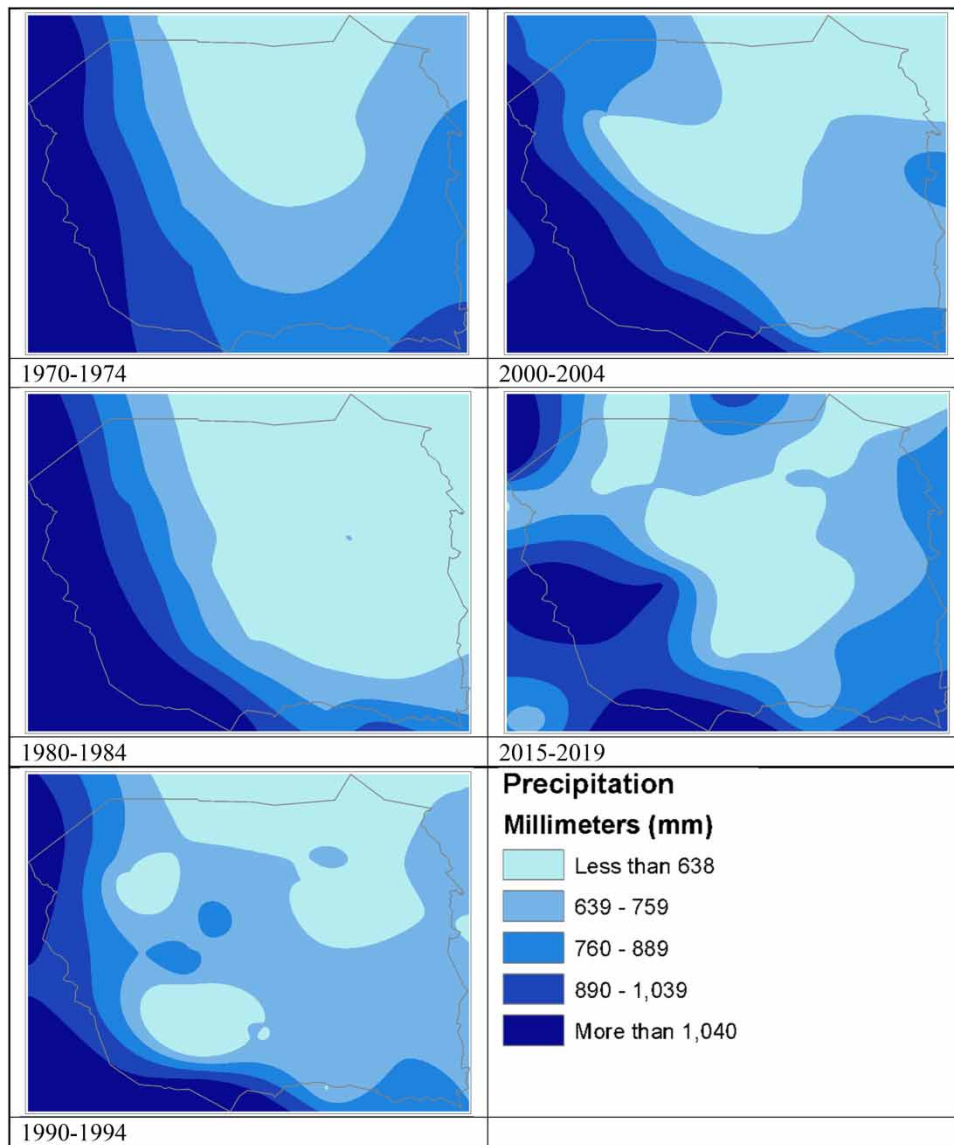
Figure 11 | The average annual precipitation for the selected 5-year periods.

observed, probably related to climatic variations, such as temperature, as reported in SACMEX (2005); also, as seen in Figure 14, the estimated PR slightly follows the precipitation pattern. For the 40 years, while urban surface increased from 16 to 28%, the potential recharge diminished from 23 to 19% in the same period.

According to Figure 14, urbanization plays an important role in the percentage of PR. While in the period 2005–2009, where there was a considerable increase in precipitation, its effect on the trajectory of the percentage of PR seems only to level it, in 2015–2019, there was also a slight increase in precipitation, but the percentage of PR is more notably affected by the increase in urbanization. Of course, this is for the percentage of PR in the whole SBM, but precipitation influence might be more significant by analyzing each PR region separately. Also, Table 9 shows the results of estimated infiltrated volumes in Mm³/year. Note that the first period with the highest precipitation infiltrated percentage may suggest a correlation with the urbanization surface percentage for the same period. The precipitation volume varies in a range of 3017.89–3,540.81 Mm³/year corresponding to 1990–1994 and 2005–2009, respectively. While the potential recharge varies from 24% (823.71 Mm³/year) to 19% (630.83 Mm³/year) of precipitation, corresponding to 1975–1979 and 2015–2019,
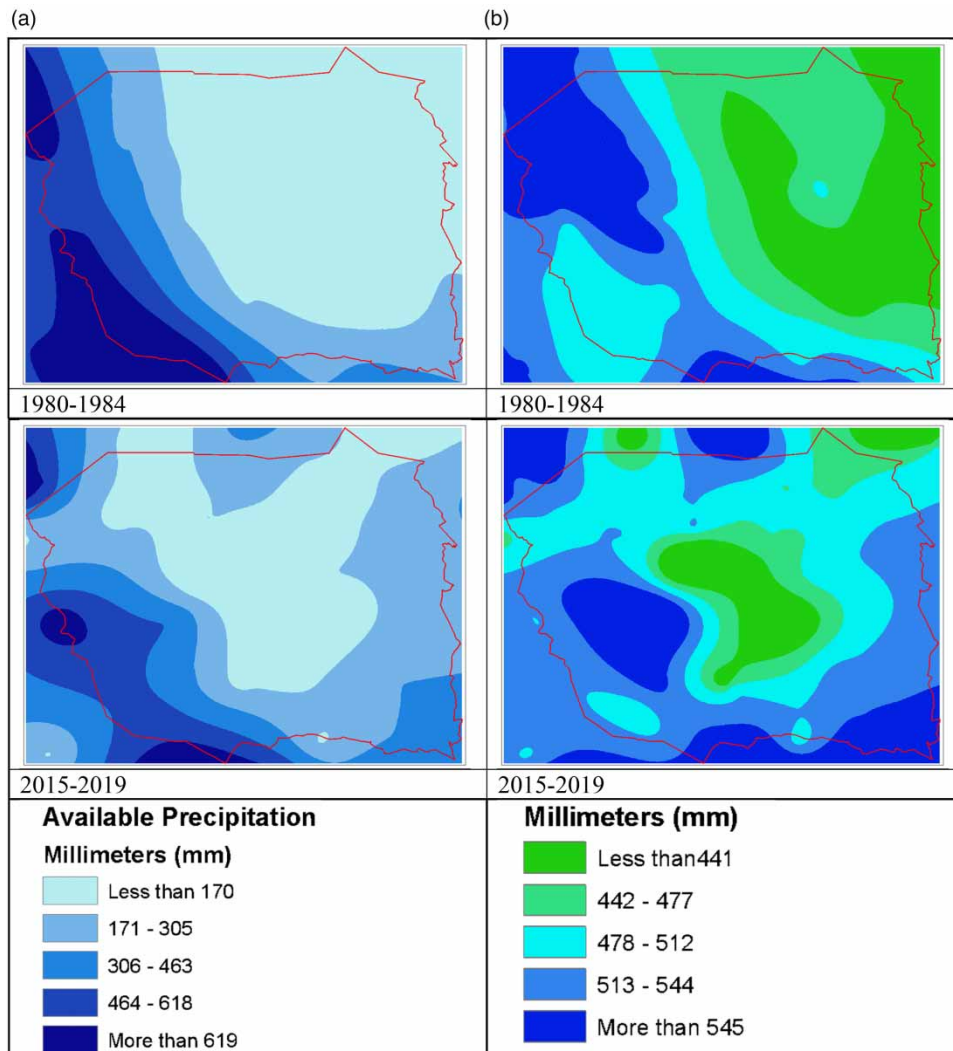
Figure 12 | (a) Calculated available precipitation. (b) Calculated real evapotranspiration (Turc method).

respectively, representing a maximum decrease of 24% in potential recharge. This result is close to the Peña-Díaz (2019) result of 647 Mm³/year, but his study was for the entire Valley of Mexico from 1980 to 2011.

In a previous study (SACMEX 2005), the resulting mean recharge for the area was 12.3 m³/s; this value is close to that obtained in this study for the poor PR region, but the study only accounted for the ZMCM aquifer. The total area used in that study was 1,906.05 km², representing only 57% of the area considered in this work. They also reported an annual volume estimated on average for aquifer recharge of 274.7 Mm³/year. Meanwhile CONAGUA (2015) officially reported 512.8 Mm³/year (which is equivalent to 16 m³/s), for the principal aquifer of the metropolitan zone (ZMCM). The mean value of PR (including all 5-year periods shown in Table 9) has a gross average of 682 Mm³ or 22 m³/s, which is not too far from that officially reported, considering that it was calculated for the three administrative aquifers in the SBM.

The variation observed in the results for the potential recharge shows a dependency on the input data and the hydrological information since they present a high variation instead of unique values, especially if they are analyzed on small scales. In this sense, the balance equation estimates PR as the complement of the other flows involved in the hydrological cycle that are more easily measured or estimated. However, given this uncertainty, the PR is more feasible as a realistic range instead of an exact value that satisfies the objectives of this study. This confirms the importance of accurately estimating a model's parameters, as indicated by other authors, since using more complex models introduces more significant errors and variations in estimating the water balance components (De Silva 2005).
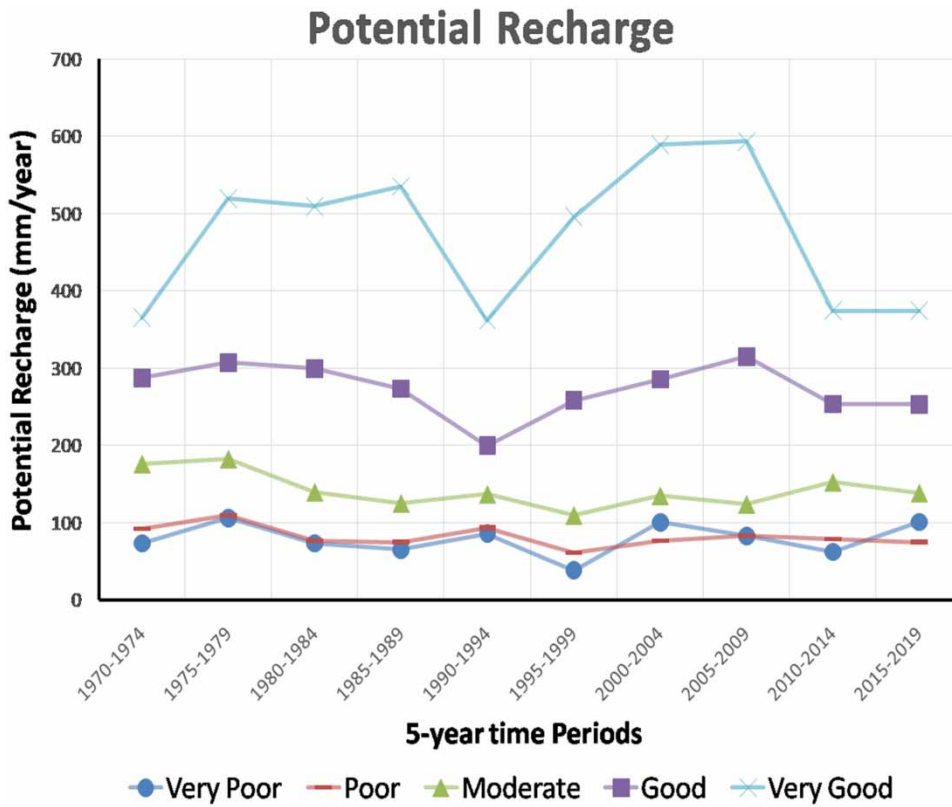
Figure 13 | Calculation of the infiltrated volume for each PR region.

Table 9 | Results of estimated infiltrated and precipitated volumes for every 5 years

Period	PR volume (Mm³/year)	Precipitation volume (Mm³/year)	Urban surface (ha)	Urban surface (%)	PR volume (%)
1970–1974	743.62	3,175.86	64,089	16	23
1975–1979	823.71	3,456.34	65,936	16	24
1980–1984	703.33	3,228.98	66,837	16	22
1985–1989	657.59	3,197.58	80,298	20	21
1990–1994	598.29	2,987.72	97,430	24	20
1995–1999	592.75	3,014.18	100,734	25	20
2000–2004	695.25	3,453.46	105,265	26	20
2005–2009	718.88	3,562.66	106,104	26	20
2010–2014	657.71	3,135.31	106,776	26	21
2015–2019	630.83	3,244.01	115,197	28	19

CONCLUSIONS

This study developed a conceptual model of recharge processes and a methodology to estimate potential recharge volumes considering its temporal changes. The methodology separates the long-time varying parameters to produce a potential recharge zoning from those that vary in a short time. This separation facilitates using the potential recharge results for the groundwater recharge calibration in a spatially distributed groundwater model. The methodology is applied in the estimation of PR in the SBM aquifer. The methodology mainly consists of collecting, processing, and analyzing georeferenced thematic data using GIS software. Geographical data, such as geological alignments, drainage networks, lithology, land use,
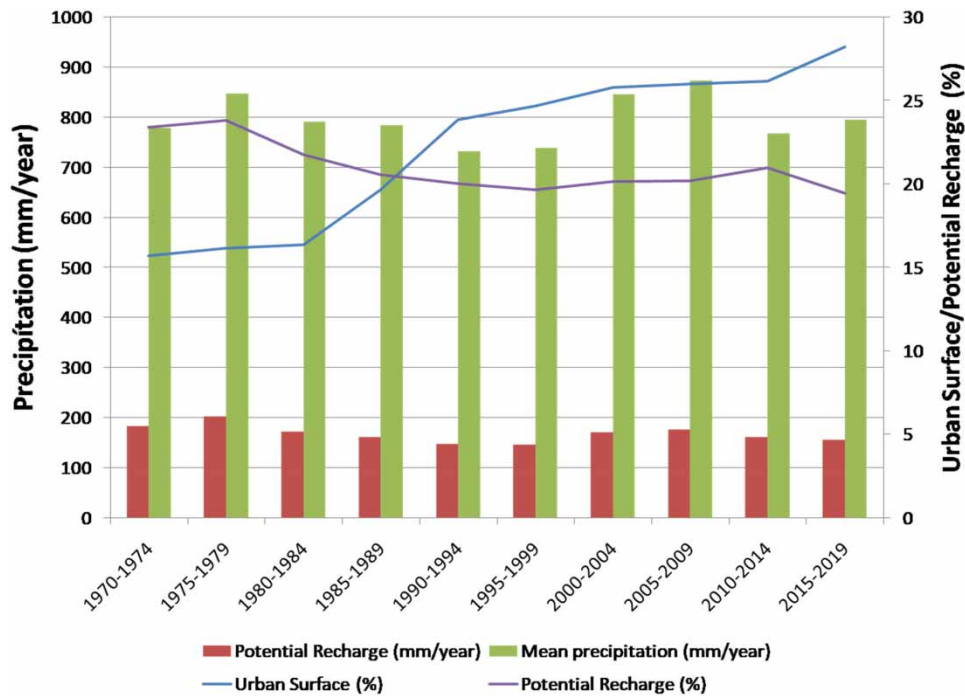
Figure 14 | Results of mean precipitation, potential recharge, and urbanized area for each analyzed period. Please refer to the online version of this paper to see this figure in colour: https://dx.doi.org/10.2166/nh.2023.103.

topography, and precipitation, define PR regions. Short-time variables and their maps were generated in intervals of 5 years along the period 1970–2019 to evaluate the evolution of potential recharge relative to the dynamic processes over time that generates it. The potential recharge is then estimated using a surface water budget equation at each PR region.

The mapped areas with the most significant recharge potential resulted in the highlands, mainly the Sierra de las Cruces and Chichinautzin, where precipitation and lithology favor potential recharge. On the other hand, the areas with the lowest potential recharge correspond to the valley, where the urban development is placed, especially those areas or neighborhoods with high population density (according to Landsat image reclassification), and the underlying ancient lakebed in the plain areas turned into a clay aquitard with low permeability significantly reduces the potential recharge.

This study proves that potential recharge depends on several critical factors. Although a higher sensibility was observed for changes in precipitation, another sensible parameter was the size of PR surfaces (considered with slightly more impact when analyzing the water budget equation by PR regions separately). In third place, the runoff coefficient depending on LUCC was found sensible, especially using values close to 1. Although several works consider a low urban impact in the total recharge, this work proves that it can be significant in highly urbanized areas. Analyzing the whole SBM surface, urban change significantly influenced PR.

Results also showed slight increases in potential recharge at some periods; this increase may confirm the results reported in SACMEX (2005) regarding the influence of temperatures. With a different behavior in the more recent periods, where a slight decrease in recharge was observed compared to earlier periods, temperatures may also play a role in conjunction with changes in land cover, urbanization, and even global warming.

In this analysis, other non-natural potential recharge sources, such as irrigation returns, leaks from the hydraulic and drainage network, reservoir recharge, and conservation structures, are not included. Future works will analyze these factors. The results can be used as input data to feed a numerical groundwater model for the SBM area. Finally, this study also deals with the sensitivity of the parameters, as shown by the potential recharge results, with the differences between urban and non-urban analyzed regions.

The limitations of the estimations presented in this work are commonly observed in any water budget, such as the precision of the input data and the understanding of the hydrological processes of a study area is defined using information from other

studies and introduces uncertainty in the calculations. Also, the time scale with which the variables that change in a short time were analyzed (5-year periods) depended on the available satellite information. The periodicity of satellite information may limit the applicability of the proposed methodology in studies that need to reflect more dynamic changes. These drawbacks constitute a focus point for future work. In addition, the results of this work may be used as a complement for a more complete analysis through the use of numerical models that solve the balance equations that describe the hydrological processes in the saturated zone and in the interface between surface water bodies and the saturated zone.

ACKNOWLEDGEMENTS

DATA AVAILABILITY STATEMENT

All relevant data are included in the paper or its Supplementary Information.

CONFLICT OF INTEREST

The authors declare there is no conflict.

REFERENCES

Adhikari, R. K., Mohanasundaram, S. & Shrestha, S. 2020 Impacts of land-use changes on the groundwater recharge in the Ho Chi Minh City, Vietnam. *Environmental Research* **185**, 1–10. doi:10.1016/j.envres.2020.109440.

Arce, J. L., Layer, P. W., Macías, J. L., Morales-Casique, E., García-Palomo, A., Jiménez-Domínguez, F. J., Benowitz, J. & Vásquez-Serrano, A. 2019 Geology and stratigraphy of the Mexico Basin (Mexico City), central Trans-Mexican Volcanic Belt. *Journal of Maps* **15** (2), 320–332. doi:10.1080/17445647.2019.1593251.

Biehl, L. & Landgrebe, D. 2002 MultiSpec – a tool for multispectral-hyperspectral image data analysis. *Computers and Geosciences* **28** (10), 1153–1159. doi:10.1016/S0098-3004(02)00033-X.

Boyás Martínez, E., González Mora, M. F. & Paredes-Tavares, J. 2021 Determinación de sitios potenciales de recarga artificial de agua subterránea en cinco acuíferos de la Zona Metropolitana del Valle de México. *Cuadernos Geográficos* **60** (3), 73–94. doi:10.30827/cuadgeo.v60i3.16226.

BuhayBucton, B. G., Shrestha S, K. C. S., Mohanasundaram, S., Virdis, S. G. P. & Chaowiwat, W. 2022 Impacts of climate and land use change on groundwater recharge under shared socioeconomic pathways: a case of Siem Reap, Cambodia. *Environmental Research* **211**, 1–33. doi:10.1016/j.envres.2022.113070.

California Waterboards 2011 *The Clean Water Team Guidance Compendium for Watershed Monitoring and Assessment, State Water Resources Control Board 5.1.3 FS-(RC) 2011*. Available from: https://www.waterboards.ca.gov (accessed February 2023).

Carrera-Hernández, J. J. & Gaskin, S. J. 2008 Spatio-temporal analysis of potential aquifer recharge: application to the Basin of Mexico. *Journal of Hydrology* **353** (3–4), 228–246. doi:10.1016/j.jhydrol.2008.02.012.

CLICOM 2021 *Base de datos climatológica nacional, Sistema CLICOM*. Consultada Febrero de 2021. Available from: http://clicom-mex.cicese.mx/

CONAGUA 2015 *Actualización de la disponibilidad media anual de agua en el acuífero Zona Metropolitana de la Cd. de México (0901)*. Distrito Federal.

De Silva, R. P. 2005 Limitations of a soil water budgeting method in estimating groundwater recharge with particular reference to the dry zone of Sri Lanka. *Journal of the National Science Foundation of Sri Lanka* **33** (2), 99–113.

Ghimire, U., Shrestha, S., Neupane, S., Mohanasundaram, S. & Lorphensri, O. 2021 Climate and land-use change impacts on spatiotemporal variations in groundwater recharge: a case study of the Bangkok area, Thailand. *Science of the Total Environment* **792**. doi:10.1016/j.scitotenv.2021.148370.

Goepel, K. D. 2013 Implementing the analytic hierarchy process as a standard method for multi-criteria decision making in corporate enterprises – a new AHP excel template with multiple inputs. In: *Proceedings of the International Symposium on the Analytic Hierarchy Process*, 2013, Kuala Lumpur, pp. 1–10. doi:10.13033/isahp.y2013.047.

Goepel, K. D. 2018 Implementation of an online software tool for the analytic hierarchy process (AHP-OS). *International Journal of the Analytic Hierarchy Process* **10** (3), 469–487. doi:10.13033/ijahp.v10i3.590.

Gómez-Reyes, E. 2013 Valoración de las componentes del balance hídrico usando información estadística y geográfica: la cuenca del Valle de México. *Revista Internacional de Estadística y Geografía* **4** (3), 4–27.

Guerrero-Morales, J., Fonseca, C. R., Goméz-Albores, M. A., Sampedro-Rosas, M. L. & Silva-Gómez, S. E. 2020 Proportional variation of potential groundwater recharge as a result of climate change and land-use: a study case in Mexico. *Land* **9** (10), 1–22. doi:10.3390/land9100364.

Healey, R. W. & Scanlon, B. R. 2010 Groundwater recharge. In: *Estimating Groundwater Recharge*. Cambridge University Press, Cambridge, pp. 1–14. doi:10.1017/CBO9780511780745.002.

Healy, R. W., Winter, T. C., LaBaugh, J. W. & Franke, O. L. 2007 *Water Budgets: Foundations for Effective Water-Resources and Environmental Management*. U.S. Geological Survey Circular, Vol. 1308. U.S. Geological Survey, Reston, VA, p. 90. https://pubs.usgs.gov/circ/2007/1308/pdf/C1308_508.pdf

Mautner, M. R. L., Foglia, L., Herrera, G. S., Galán, R. & Herman, J. D. 2020 Urban growth and groundwater sustainability: evaluating spatially distributed recharge alternatives in the Mexico City Metropolitan Area. *Journal of Hydrology* **586**, 124909. doi:10.1016/j.jhydrol.2020.124909.

Merlos-Villegas, F., Sánchez-Quispe, S. T. & Almanza-Campos, J. A. 2014 Creación de un sistema de información hidrológico para el cálculo de intensidades máximas y gestión de datos meteorológicos. In *XXIII Congreso Nacional De Hidráulica Puerto Vallarta*, Octubre 2014, Jalisco, México. AMH, Puerto Vallarta, pp. 1–8.

Oikonomidis, D., Dimogianni, S., Kazakis, N. & Voudouris, K. 2015 A GIS/remote sensing-based methodology for groundwater potentiality assessment in Tirnavos area, Greece. *Journal of Hydrology* **525**, 197–208. doi:10.1016/j.jhydrol.2015.03.056.

Ortega, A. & Farvolden, R. N. 1989 Computer analysis of regional groundwater flow and boundary conditions in the basin of Mexico. *Journal of Hydrology* **110**, 271–294.

Osorio, J. & Orejuela, J. 2008 EL proceso de Análisis Jerárquico (AHP) y la toma de decisiones multicriterio. Ejemplo de aplicación. *Scientia et Technica* **XIV** (39), 247–252.

PAOT 2009 *Diagnóstico de las zonas afectadas por la tala clandestina y la presión urbana dentro de las tres anp y propuesta de y propuesta de recomendaciones para su manejo, recomendaciones para su manejo, conservación y aprovechamiento sustentable*. Procuraduría Ambiental y Del Ordenamiento Territorial del D.F., Mexico, D.F

Peña-Díaz, S. 2019 Water conditions in the Valley of Mexico Basin. *Tecnologia y Ciencias del Agua* **10** (2), 98–127. doi:10.24850/j-tyca-2019-02-04.

Peng, Z. 2019 Estimating daily inflows of large lakes using a water-balance-based runoff coefficient scaling approach. *Hydrological Processes* **33**, 2535–2550. doi:10.1002/hyp.13486.

Ruiz, G. 2015 Estimation of the groundwater recharge in the aquifer of the Mexico city. *Procedia Environmental Sciences* **25**, 220–226. doi:10.1016/j.proenv.2015.04.030.

Rwanga, S. S. & Ndambuki, J. M. 2017 Approach to quantify groundwater recharge using GIS based water balance model: a review. *International Journal of Research in Chemical, Metallurgical and Civil Engineering* **4** (1). doi:10.15242/ijrcmce.ae0317115.

Saaty, T. L. 1990 How to make a decision: the analytic hierarchy process. *European Journal of Operational Research* **48** (1), 9–26. doi:10.1016/0377-2217(90)90057-I.

Salas, J. D., Yevjevich, V. & Lane, W. L. 1980 *Applied Modeling of Hydrologic Time Series*. Water Resources Publications, Colorado.

Sánchez-Quispe, S. T., Navarro-Farfán, M. d. M. & García-Romero, L. 2021 *Methodology for Processing Meteorological and Hydrometric Data at Basin*. En: ECORFAN, ed. CIERMMI Women in Science TXVI Engineering and Technology. Handbooks-©ECORFAN-México, Querétaro, pp. 107–145.

Sistema de Aguas de la Ciudad de México (SACMEX) 2005 *Estudio para obtener la disponibilidad del acuífero de la zona metropolitana de la ciudad de México, Contrato No. 06-CD-03-1O-0267-1-05*. Instituto Mexicano de Tecnologia del Agua, México, D.F

Son, J. & Kwon, T. 2022 Evaluation and improvement measures of the runoff coefficient of urban parks for sustainable water balance. *Land* **11** (1098), 1–20. doi:10.3390/land11071098.

Suganthi, S., Elango, L. & Subramanian, S. K. 2013 Groundwater potential zonation by remote sensing and GIS techniques and its relation to the groundwater level in the coastal part of the Arani and Koratalai river basin, Southern India. *Earth Sciences Research Journal* **17** (2), 87–95.

Wang, H., Kgotlhang, L. & Kinzelbach, W. 2008 Using remote sensing data to model groundwater recharge potential in Kanye Region, Botswana. *The International Archives of the Photogrammetry, Remote Sensing and Spatial Information Sciences* **37** (B8), 751–756.